NACA RM L55A24a

NACA

RESEARCH MEMORANDUM

PRELIMINARY RESULTS OF AN INVESTIGATION AT TRANSONIC SPEEDS TO DETERMINE THE EFFECTS OF A HEATED PROPULSIVE JET ON THE DRAG CHARACTERISTICS OF A RELATED SERIES OF AFTERBODIES

By Beverly Z. Henry, Jr., and Maurice S. Cahn

Langley Aeronautical Laboratory
Langley Field, Va.

NATIONAL ADVISORY COMMITTEE
FOR AERONAUTICS

WASHINGTON

March 25, 1955
Declassified May 29, 1959

NACA RM L55A24a

NATIONAL ADVISORY COMMITTEE FOR AERONAUTICS

RESEARCH MEMORANDUM

PRELIMINARY RESULTS OF AN INVESTIGATION AT TRANSONIC SPEEDS TO DETERMINE THE EFFECTS OF A HEATED PROPULSIVE JET ON THE DRAG CHARACTERISTICS OF A RELATED SERIES OF AFTERBODIES

By Beverly Z. Henry, Jr., and Maurice S. Cahn

SUMMARY

An investigation has been conducted at transonic speeds to determine the effects of a sonic propulsive jet on the body from which it issues as influenced by changes in afterbody geometry. Preliminary results of the investigation are presented herein with limited analysis.

These results indicate that the effects of a jet would be favorable on bodies of lower boattail angle (7.7°, 16°, and 24°) and unfavorable on bodies of higher boattail angle (45°). Increasing the base-annulus size of a body of favorable boattail angle caused no appreciable change in the trend of favorable jet effects for the range of base-annulus sizes considered. In most cases increasing the jet temperature caused a reduction in afterbody pressure drag. The influence of stream Mach number varied. The jet effects tended to show no change or to decrease slightly with increasing Mach number for the low boattail angles and to increase with increasing Mach number for high boattail angles.

INTRODUCTION

With the rapid increase in the use of jet propulsion systems, adequate information concerning the effects of propulsive jets on the aerodynamic characteristics of the bodies from which they issue has not been available. This lack of information is particularly critical at the present time in the transonic speed range since, from the standpoint of range and economy, even those designs capable of supersonic speeds are required to cruise in the high subsonic region.

An investigation has been conducted in the Langley 8-foot transonic tunnel to evaluate some of the effects of a sonic propulsive jet as

influenced by changes in afterbody geometry. The investigation was conducted at an angle of attack of 0° through the Mach number range from 0.80 to 1.10, and at each point the jet temperature and pressure ratio were varied.

Presented in this report are the basic data obtained from the investigation. The data are presented with limited analysis in order to expedite their availability to those concerned with jet-exit—afterbody design.

SYMBOLS

A	area
C_D	drag coefficient, $\sum \frac{P_l A_l}{A_m}$
H	total pressure
L	length
M	Mach number
P	pressure coefficient, $\frac{p_l - p_o}{q_o}$
R	Reynolds number, based on body length
T	total temperature, °F
d	diameter
p	static pressure
q	dynamic pressure, $\frac{\gamma}{2} pM^2$
β	afterbody boattail angle, deg
γ	ratio of specific heats

Subscripts:

A	afterbody
b	base

j	jet
0	free stream
β	boattail
l	local
m	model

APPARATUS AND TESTS

Wind tunnel.- This investigation was conducted in the Langley 8-foot transonic tunnel which has a dodecagonal, slotted test section and permitted continuous testing up to a Mach number of approximately 1.10 for these models. The tunnel is vented to the atmosphere through an air exchange tower which permitted the exhausting of combustion gasses from the model into the stream with no detrimental effects on the characteristics of the stream. Details of the test section are presented in reference 1. Aerodynamic characteristics of the airstream are given in reference 2 wherein it is shown that the maximum deviation from the indicated free-stream Mach number is ± 0.003.

Models.- The models used in the investigation were bodies of revolution, the rear portions of which were removed to provide an exit for the jet. These bodies had fineness ratios from 10.0 to 10.7. A single forebody was used throughout the investigation and the model design allowed the ready interchange of afterbodies of various geometric shape. The models were mounted in the tunnel by means of two support struts. These support struts, with a chord of 11.25 inches and an NACA 65-010 airfoil section measured parallel to the airstream were placed so that the leading edge intersected the body at a point 21.7 inches from the nose and were swept back 45°. A sketch of the general arrangement of the model in the tunnel is presented in figure 1. For all tests the nose of the model was located 46 inches downstream of the slot origin. The models were instrumented with three rows of static-pressure orifices at 0°, 45°, and 72° from the plane of symmetry and with base pressure orifices.

Presented in table I is the equation utilized to define the external shapes of the afterbodies investigated, with the exception of afterbody IX. Also shown are the design points used to assign values to the equation. Tabulated in table II are the ordinates from which the body shapes were constructed. Drawings of the afterbody shapes are shown in figure 2. The formation of a body with jet-to-base diameter ratio of 1.000 (afterbody IE) was accomplished by the addition of a 16° conical extension to afterbody I.

Turbojet simulator.- Contained within the models was a device for the simulation of a turbojet exhaust (see fig. 3(a)). To satisfy the simulation requirements, a combustor was developed which burns a mixture of ethylene and air and exhausts the combustion products through a sonic nozzle. The burning of such a mixture produces the desired physical and thermodynamic characteristics of a non-afterburning turbojet exhaust.

The turbojet simulator shown in figure 3(b) consists of an air- and fuel-distribution manifold, an electrical ignition system, a cylindrical combustion chamber, and a simple converging nozzle.

The flow of fuel and air to the simulator were remotely controlled by two sensitive, manually operated regulators. Jet pressure ratio was varied by changes in mass flow to the simulator and jet temperature was varied by changes in fuel-air ratio.

Tests and measurements.- For this investigation, the models were tested at an angle of attack of 0° through the Mach number range from 0.80 to 1.10. At each test Mach number, the jet pressure ratio was varied from a no-flow condition to 11 or to the maximum obtainable at jet temperatures of cold, 800°, and $1{,}200^\circ$ F. The term "cold" flow is used herein to define the temperature of the air coming from the source, normally 75° to 80°, and corresponds to a fuel-air ratio of 0. The jet pressure ratio for a no-flow condition is assigned a value of 1 in the presentation of the results. The Reynolds number based on body length varied from 15.0×10^6 to 17.4×10^6 (see fig. 4).

At each test point, body pressure distribution, base pressure, and all pressure data relative to prevailing ambient test conditions were photographically recorded from multiple-tube manometers. Tunnel total temperature was obtained from a recording potentiometer.

Rates of flow of fuel and air were determined by use of standard ASME sharp-edged-orifice flow meters. Jet total pressure was obtained from a calibrated probe mounted in the combustor and was referenced to a static-pressure orifice on the tunnel wall for the determination of jet pressure ratio. Jet temperature was obtained from a shielded chromel-alumel thermocouple near the exit station (see fig. 3). All values defining the jet condition were photographically recorded by a camera synchronized with that used to record pressure data.

RESULTS

The basic results of the investigation are presented in figures 5 and 6. Presented are base pressure coefficients, body boattail pressure-drag coefficients, base pressure-drag coefficients, and total afterbody

pressure-drag coefficients as a function of jet pressure ratio for various Mach numbers and at jet temperatures of cold, 800° , and 1,200° F. Attention is invited to the fact that in the presentation of data it has been found expedient to utilize shifted and broken scales. Values of afterbody pressure-drag coefficient were determined by numerical integration of body pressures and are based on body frontal area. Base pressure-drag coefficient was determined in all cases, including the no-flow condition, from the pressure acting on the base annulus area. The effects of the jet are considered as the departure from the condition of no jet flow. Very low jet pressure ratios corresponding to a base-bleed condition were not investigated and the fairing of the curves neglects these effects.

Presented in figure 5(a) are base-pressure-coefficient values for afterbodies I, II, and III which provide an indication of the influence of boattail angle at a jet-to-model diameter ratio of 0.248 and a jet-to-base diameter ratio of 0.742. A comparison of afterbodies IV, V, and VI, shown in figure 5(b), again indicates the influence of boattail angle but at a higher value of jet-to-model diameter ratio. Base pressure coefficients for afterbody IX, the shape of which is similar but not identical to one derived from the equation given in table I for a boattail angle of 7.7° , are presented in figure 5(c). Values of jet pressure ratio in excess of 5 could not be obtained for the larger jet sizes because of air-supply limitations. Afterbodies I, VII, and VIII are compared in figure 5(d) to indicate the effect of increasing the base-annulus size at constant values of boattail angle and jet-to-model diameter ratio.

In figure 6 are presented the variation of pressure-drag coefficients with jet pressure ratio. The values have been presented in component and total form to indicate the relative contribution of the boattail and the base to the total afterbody pressure drag. Separate figures have been prepared for the various afterbodies. A comparison of afterbodies I, II, and III (figs. 6(b), 6(c), and 6(d)) indicates the influence of boattail angle at a jet-to-model diameter ratio of 0.248, and a comparison of afterbodies IX, IV, V, and VI (figs. 6(e), 6(f), 6(g), and 6(h)) indicates the influence of boattail angle at a jet-to-model diameter ratio of 0.351. The influence of base-annulus size can be seen by comparison of afterbodies IE, I, VII, and VIII (figs. 6(a), 6(b), 6(i), and 6(j)).

DISCUSSION

The results herein presented (figs. 6(b) to 6(h)) indicate that, at the lower boattail angles of this investigation (7.7° , 16° , and 24°) with the jet operating at 1,200° F, the effect of increasing the jet pressure ratio is generally to lower the afterbody drag. The trend is for an initial reduction in drag as the jet pressure ratio increases to 2 followed by a leveling-out or an increase in drag as the jet

pressure ratio is increased to between 3 and 5, with further increases in jet pressure ratio resulting in decreases in drag. Increasing the boattail angle at higher Mach numbers appears to shift the jet pressure ratio at which the second drag reduction starts to higher values. At the higher boattail angle (45°) the effect of increasing the jet pressure ratio is generally unfavorable. It was noted that for afterbody III ($\beta = 45°$) flow separation occurred over approximately the rear 2 inches at all Mach numbers investigated. These trends appear to remain the same for both values of jet-to-model diameter ratio investigated with the adverse effects noted for the boattail angle of 45° being more severe for the configuration with the larger exit. The smaller range of jet pressure ratios obtainable with the large exit makes comparison at the higher pressure ratios impossible. It should be noted that the models with the larger exit have a slightly lower fineness ratio than those utilizing the small exit (10 as compared to 10.7).

With a constant boattail angle that was initially favorable from the standpoint of jet effects (16°), the jet-to-base diameter ratio was reduced by stages from 1.00 to 0.525. Increasing the base-annulus size generally resulted in no appreciable change in the trend of favorable jet effects for bodies of this boattail angle (see figs. 6(a), 6(b), 6(i), and 6(j)). It is noted, however, that for the body with jet-to-base diameter ratio of 0.525 the initial drag increase has been extended to a jet pressure ratio of about 5. It appears that further increases in base-annulus size may result in serious changes in the trend of jet effects.

In most cases the effect of an increase in jet temperature from cold to 1,200° F was to lower the afterbody drag coefficient. This reduction in some cases amounted to 0.03. The favorable trend of increasing the jet temperature was noted for all bodies with the exception of afterbody IE (fig. 6(a)) which showed an unfavorable trend at a Mach number of 1.0 and of afterbody VII (fig. 6(i)) which showed a greater reduction in afterbody drag for a jet temperature of 800° than at 1,200°. No explanation for these phenomena is apparent.

The results indicate varying influence of stream Mach number on the effects of the jet on afterbody drag coefficient. The apparent trend is for the jet effects to show no change or to decrease with increasing Mach number at the lower boattail angles and to increase with Mach number at the higher angles.

SUMMARY OF RESULTS

From the preliminary results of an investigation at transonic speeds to determine the effects of a sonic propulsive jet on the body from which it issues as influenced by changes in afterbody geometry the following observations are made:

1. The general effect of increasing the jet pressure ratio was to cause a reduction in afterbody pressure-drag coefficient for lower values of boattail angle, whereas at higher values of boattail angle, the effect was adverse.

2. For a body with a favorable boattail angle, increasing the size of the base annulus caused no appreciable change in the favorable trend of the jet effects for the range of base-annulus sizes considered.

3. In most cases the effect of an increase in jet temperature from cold to 1,200° F was to lower the afterbody pressure-drag coefficient.

4. The influence of stream Mach number varied. The trend was for the jet effects to remain essentially constant or to decrease slightly with increasing Mach number for the lower boattail angles and to increase with increasing Mach number for the higher angles.

Langley Aeronautical Laboratory,
National Advisory Committee for Aeronautics,
Langley Field, Va., January 10, 1955.

REFERENCES

1. Wright, Ray H., and Ritchie, Virgil S.: Characteristics of a Transonic Test Section With Various Slot Shapes in the Langley 8-Foot High-Speed Tunnel. NACA RM L51H10, 1951.

2. Ritchie, Virgil S., and Pearson, Albin O.: Calibration of the Slotted Test Section of the Langley 8-Foot Transonic Tunnel and Preliminary Experimental Investigation of Boundary-Reflected Disturbances. NACA RM L51K14, 1952.

TABLE I

AFTERBODY DESIGN

Equation:

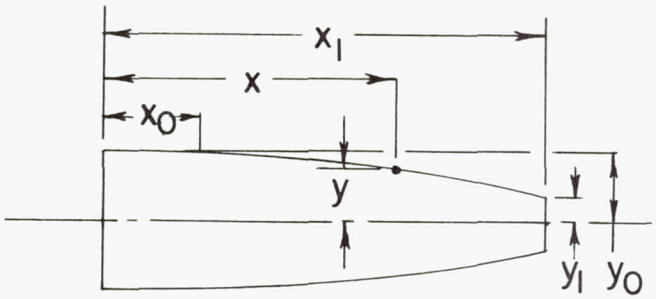

$$y = y_o - (y_o - y_1)\left(\frac{x - x_o}{x_1 - x_o}\right)\left(\frac{x_1 - x_o}{y_o - y_1}\right)\tan\beta$$

where: x = any afterbody station
x_1 = body base station
x_o = body tangency point
y = radius at station x
y_1 = body base radius
y_o = maximum body radius
β = boattail angle
$\frac{x_1 - x_o}{y_o - y_1}$ = constant

Design points:

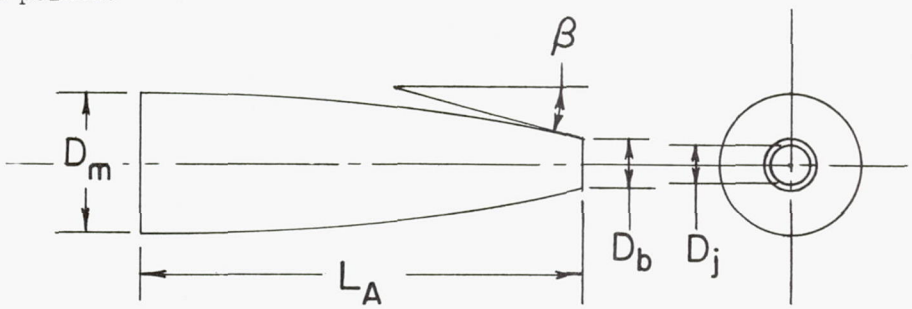

Afterbody	D_m, in.	L_A, in.	β, deg	D_j, in.	D_b, in.	D_j/D_b	D_j/D_m
IE	5.0	16.40	16	1.240	1.240	1.000	0.248
I	"	15.70	"	"	1.672	.742	"
II	"	"	24	"	"	"	"
III	"	"	45	"	"	"	"
IV	"	12.72	16	1.754	2.364	"	.351
V	"	"	24	"	"	"	"
VI	"	"	45	"	"	"	"
VII	"	15.70	16	1.240	1.930	.643	.248
VIII	"	"	"	"	2.364	.525	"
IX	"	19.55	7.7	1.754	2.513	.698	.351

TABLE II

BODY ORDINATES

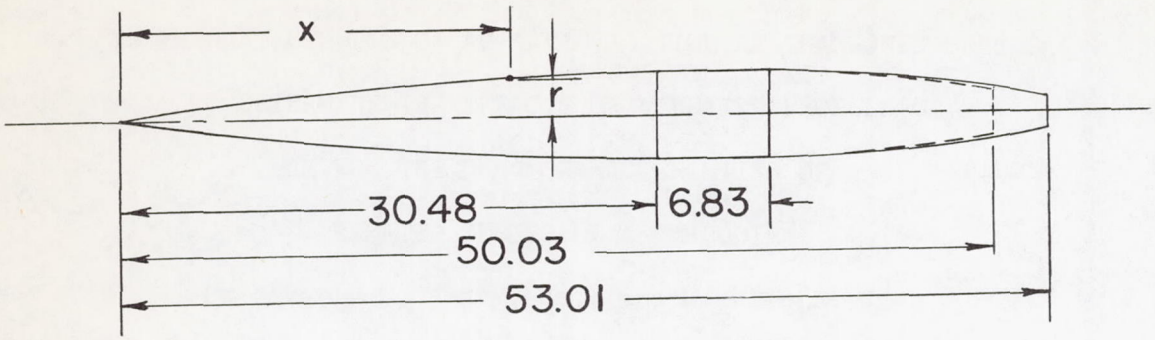

Forebody Ordinates

Sta. x, in.	Radius	Sta. x, in.	Radius
0.300	0.139	12.000	1.854
.450	.179	15.000	2.079
.750	.257	18.000	2.245
1.500	.433	21.000	2.360
3.000	.723	24.000	2.438
4.500	.968	27.000	2.486
6.000	1.183	30.000	2.500
9.000	1.556	30.480	2.500

Afterbody Ordinates

Station x, in.	Radius, r, inches								
	I	II	III	IV	V	VI	VII	VIII	IX
30.48	2.500	2.500	2.500	2.500	2.500	2.500	2.500	2.500	2.500
33.12	---	---	---	---	---	---	---	---	2.478
36.12	---	---	---	---	---	---	---	---	2.414
37.31	2.500	2.500	2.500	2.500	2.500	2.500	2.500	2.500	---
39.12	---	---	---	---	---	---	---	---	2.305
40.12	2.500	2.500	2.500	2.499	2.500	2.500	2.500	2.500	---
42.12	2.469	2.495	2.500	2.446	2.488	2.500	2.492	2.500	2.137
44.12	2.364	2.458	2.500	2.293	2.414	2.498	2.419	2.484	---
45.12	---	---	---	---	---	---	---	---	1.877
46.12	2.176	2.350	2.496	2.031	2.211	2.469	2.260	2.381	---
48.12	1.901	2.130	2.459	1.654	1.814	2.235	2.006	2.173	1.516
50.03	---	---	---	1.182	1.182	1.182	---	---	1.257
50.12	1.534	1.752	2.268	---	---	---	1.654	1.854	---
51.12	1.315	1.490	2.013	---	---	---	1.440	1.650	---
52.12	1.073	1.172	1.545	---	---	---	1.201	1.416	---
53.01	.836	.836	.836	---	---	---	.965	1.182	---

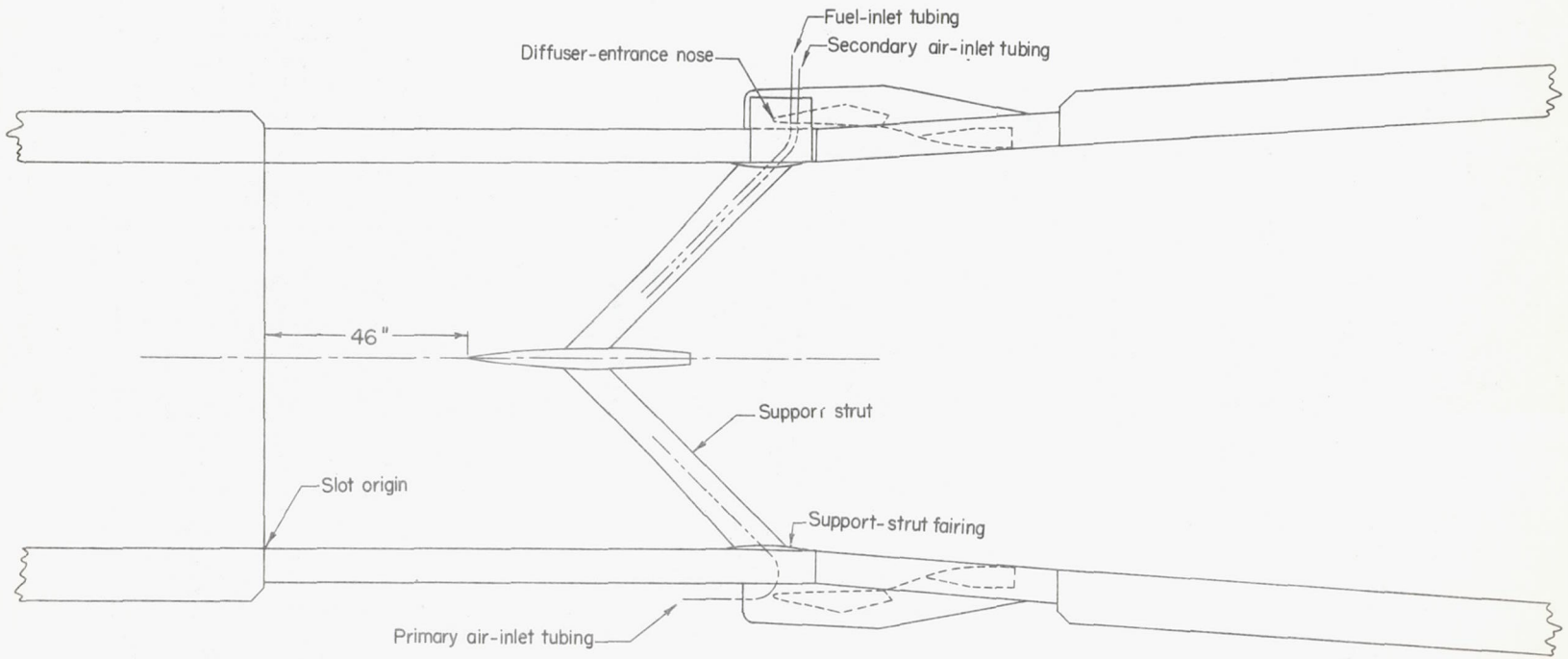

Figure 1.- Turbojet-simulator model in Langley 8-foot transonic tunnel.

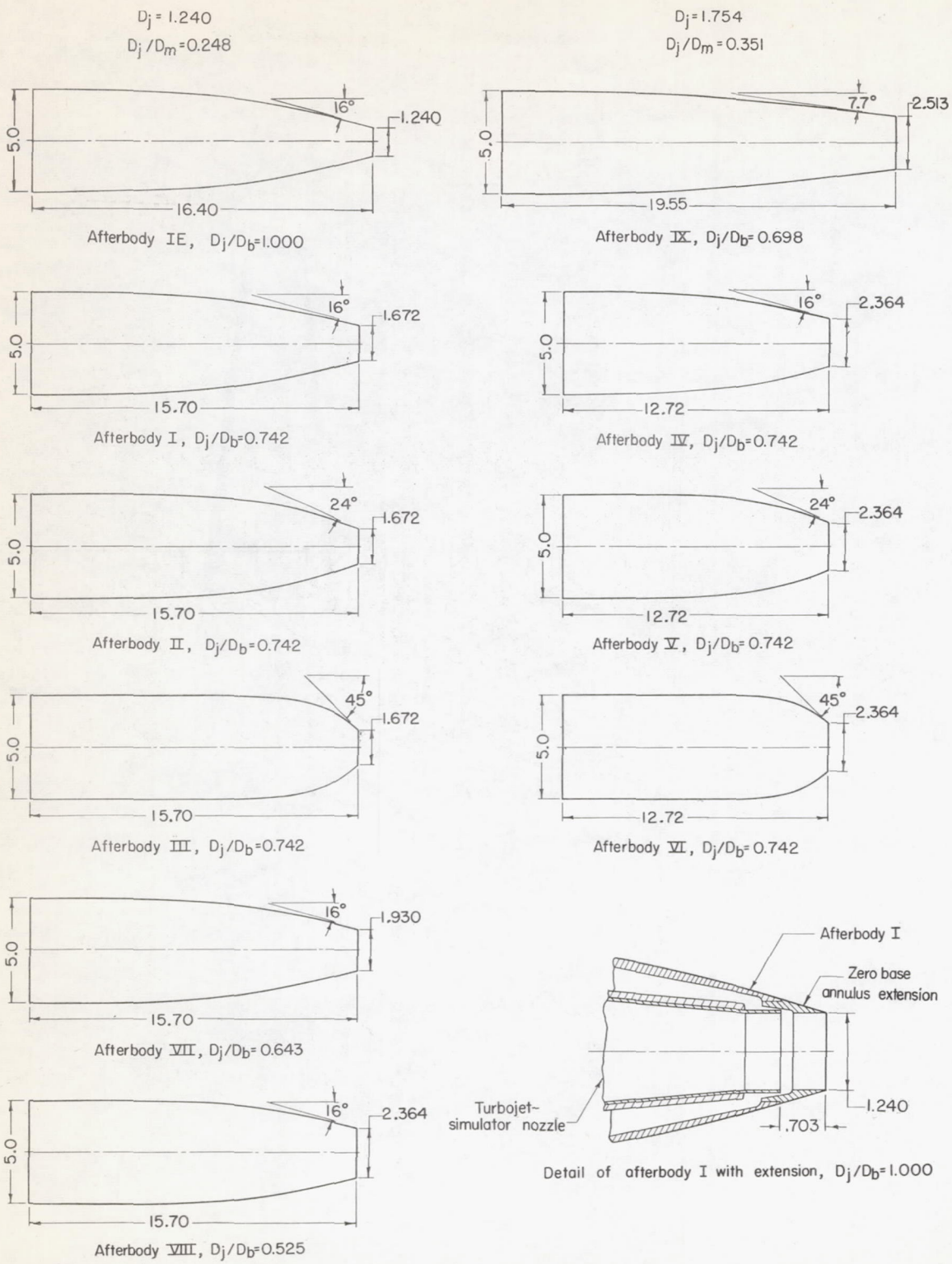

Figure 2.- Drawing of afterbody shapes investigated. All dimensions are in inches.

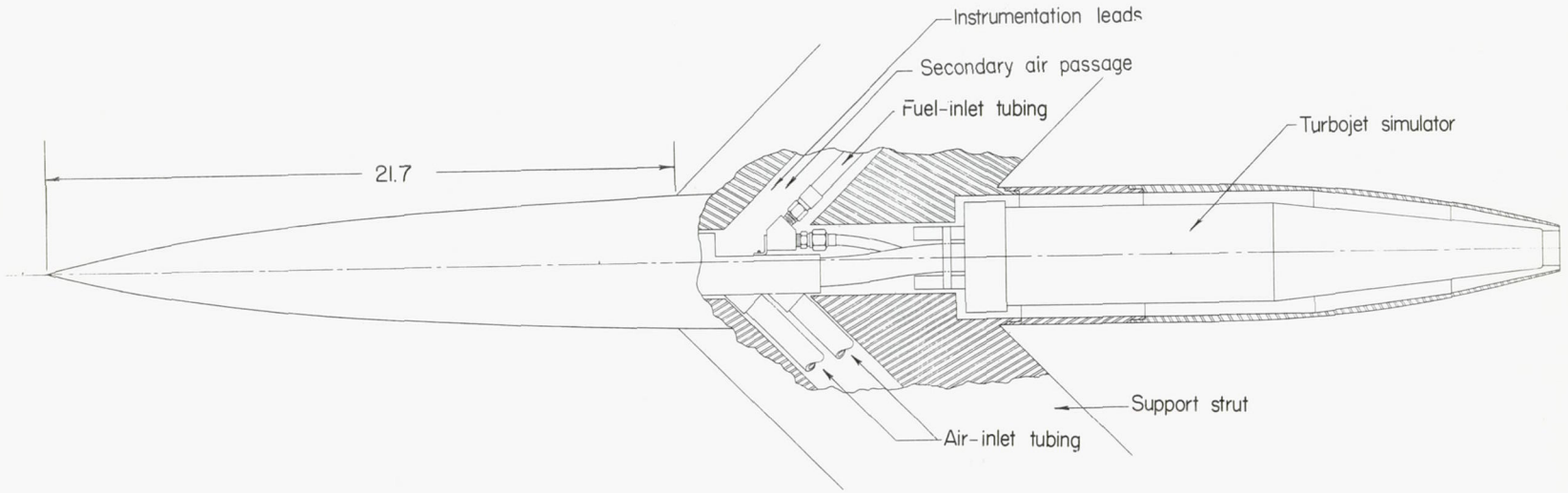

(a) Turbojet simulator installed in model.

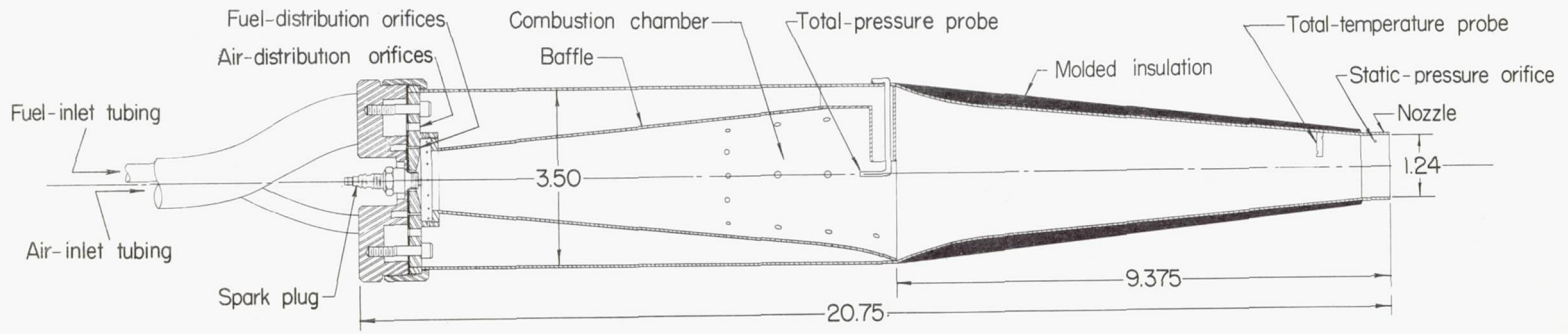

(b) Details of turbojet simulator.

Figure 3.- Drawing of model and turbojet-simulator installation. All dimensions are in inches.

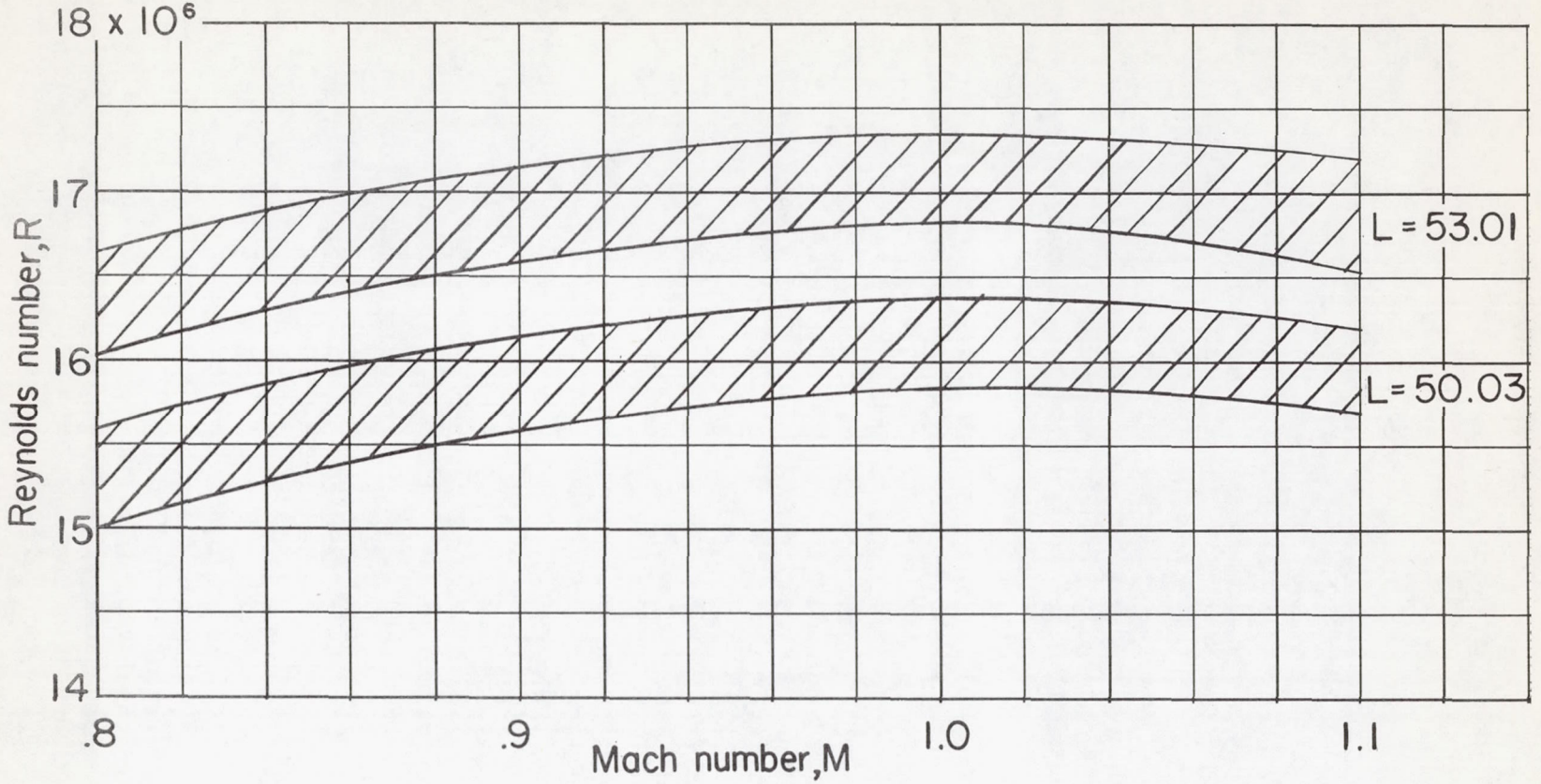

Figure 4.- Variation of Reynolds number, based on body length, with Mach number.

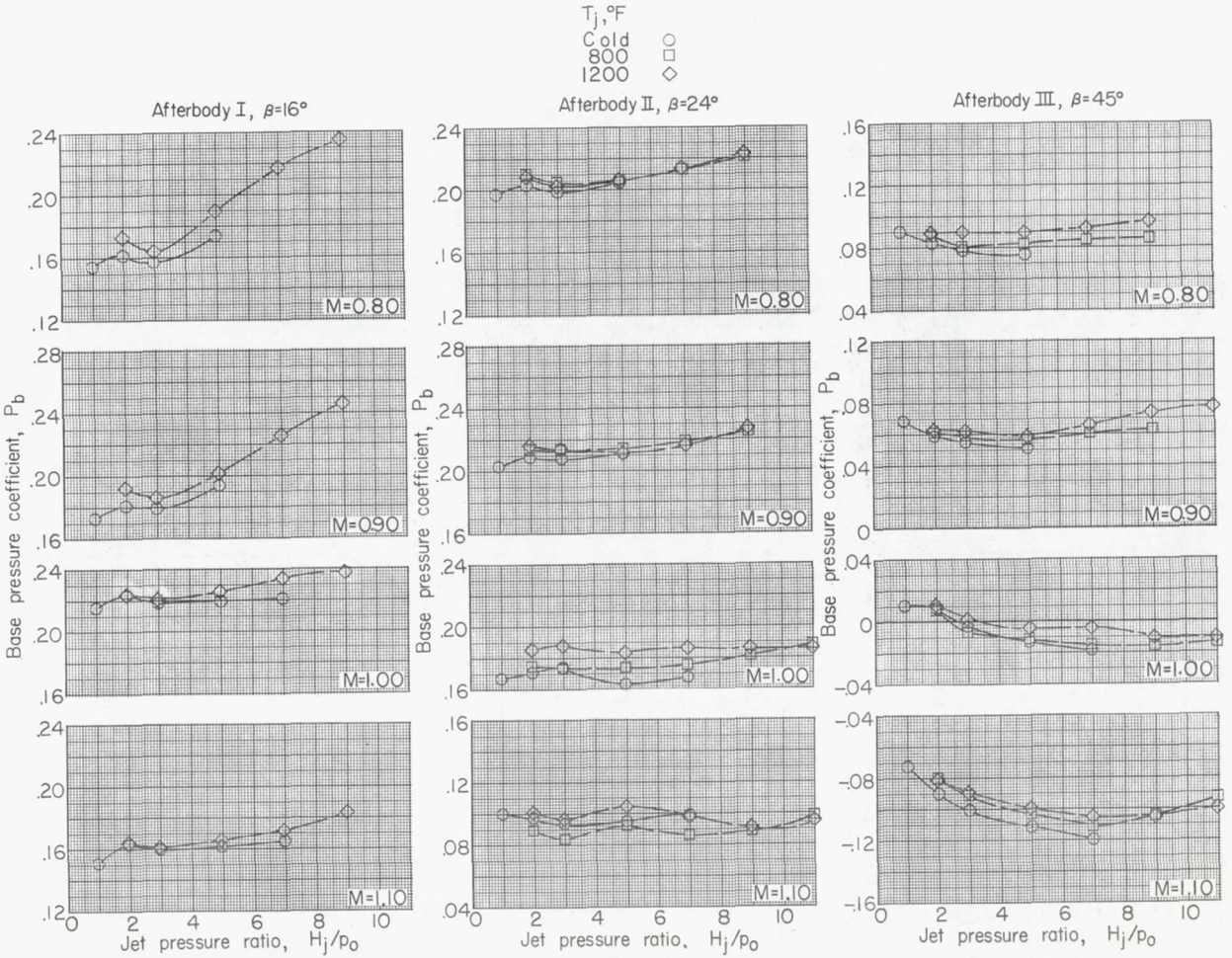

(a) Afterbodies I, II, and III. $D_j/D_m = 0.248$; $D_j/D_b = 0.742$.

Figure 5.- Variation of base pressure coefficient with jet pressure ratio at different values of jet temperature and stream Mach number.

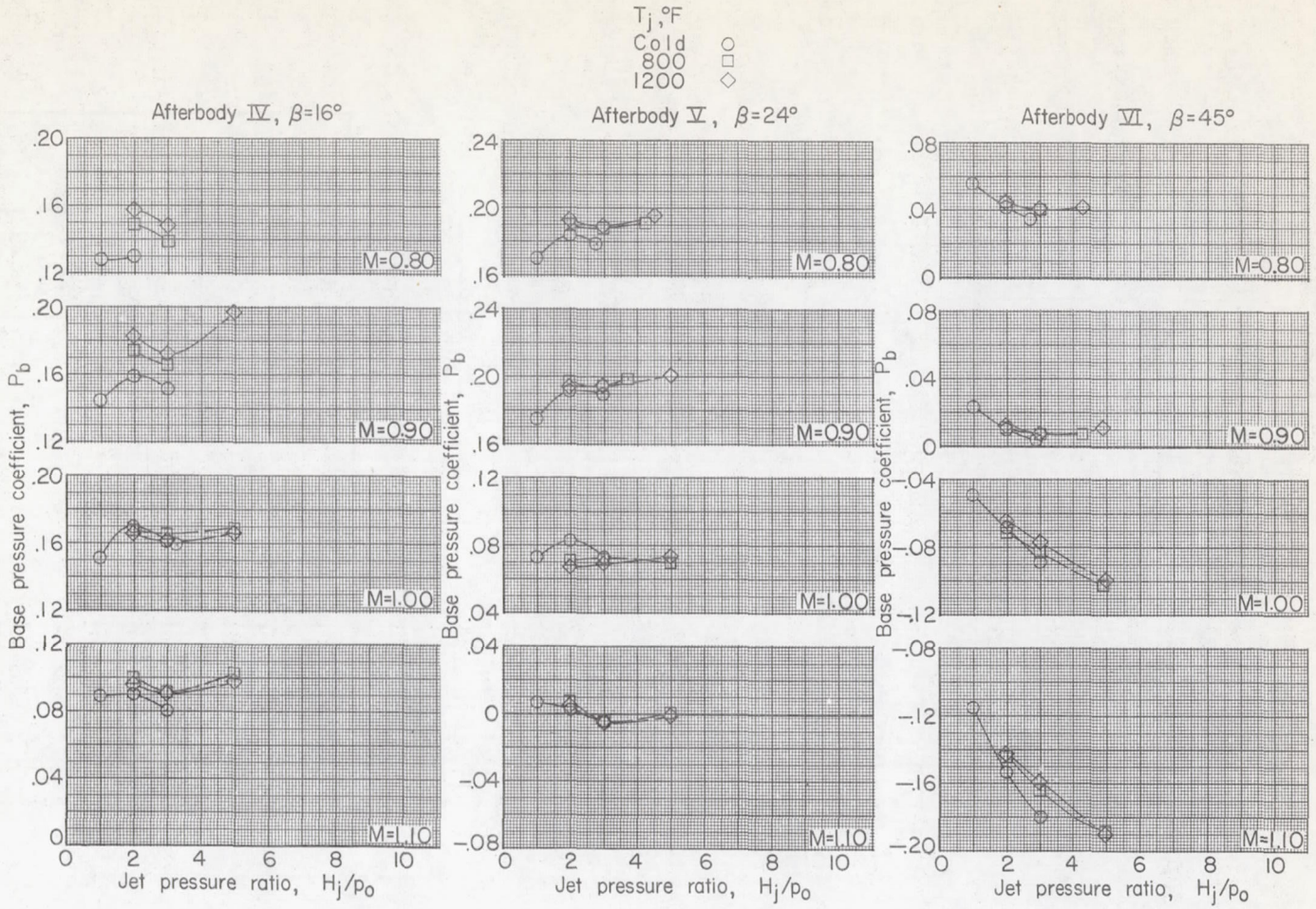

(b) Afterbodies IV, V, and VI. $D_j/D_m = 0.351$; $D_j/D_b = 0.742$.

Figure 5.- Continued.

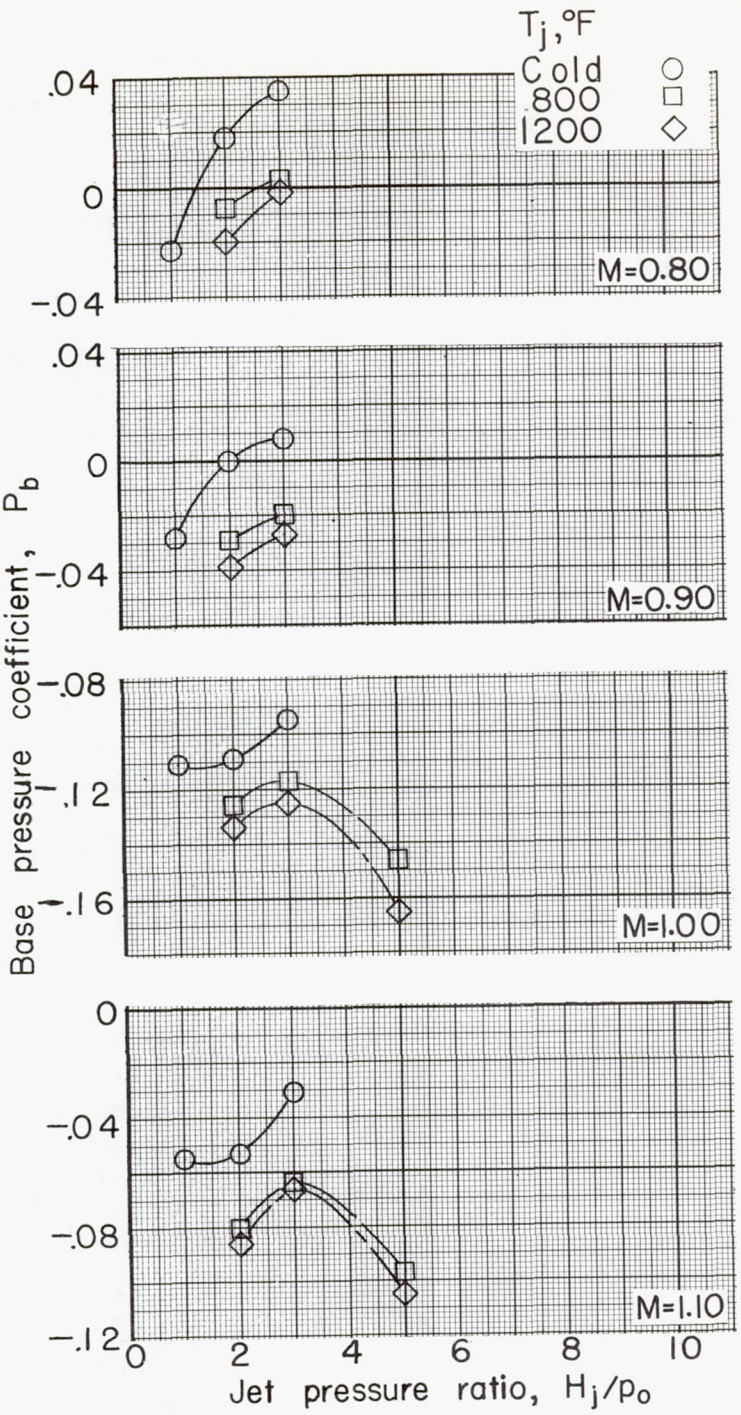

(c) Afterbody IX. $D_j/D_m = 0.351$; $D_j/D_b = 0.698$.

Figure 5.- Continued.

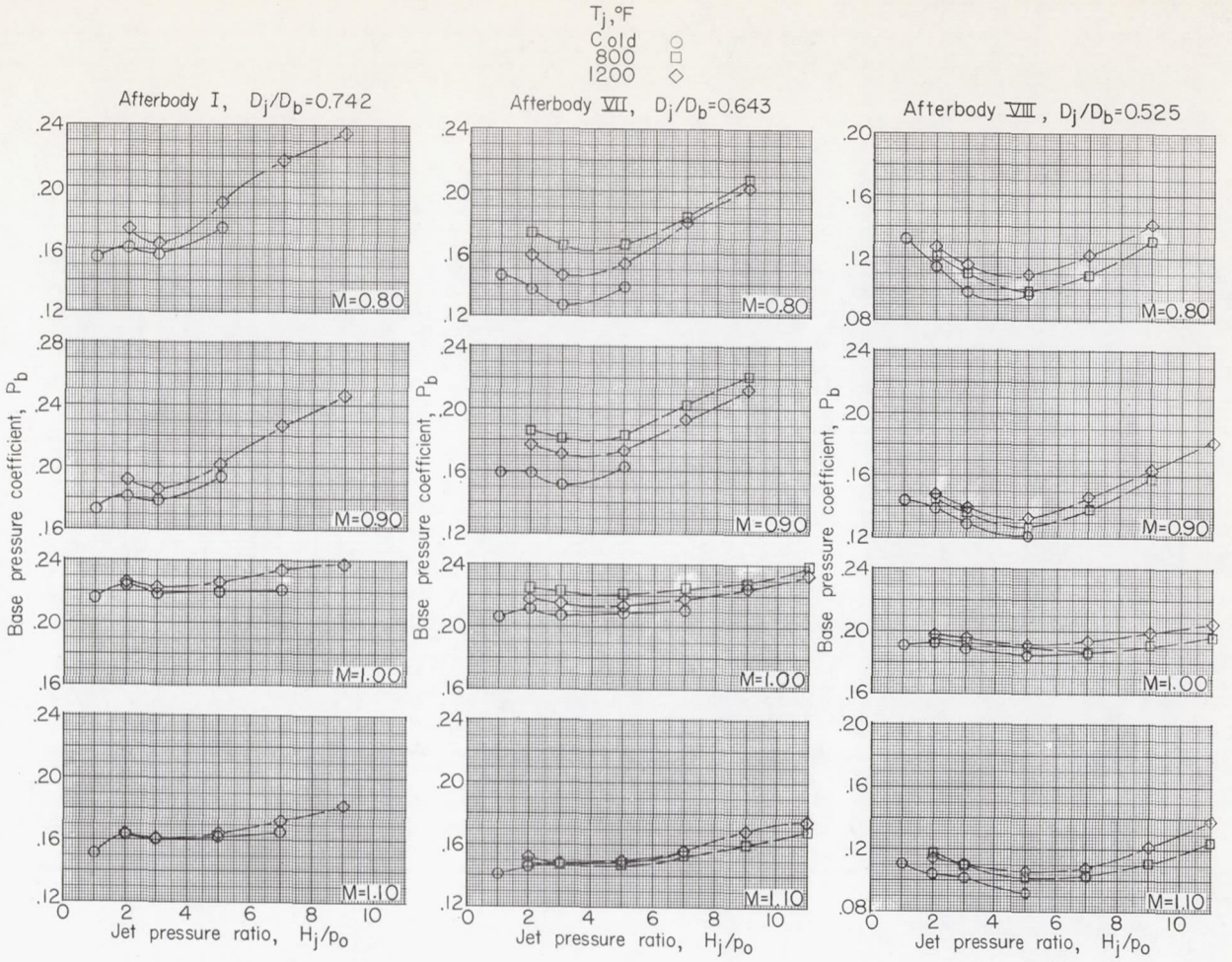

(d) Afterbodies I, VII, and VIII. $D_j/D_m = 0.248$; $\beta = 16^\circ$.

Figure 5.- Concluded.

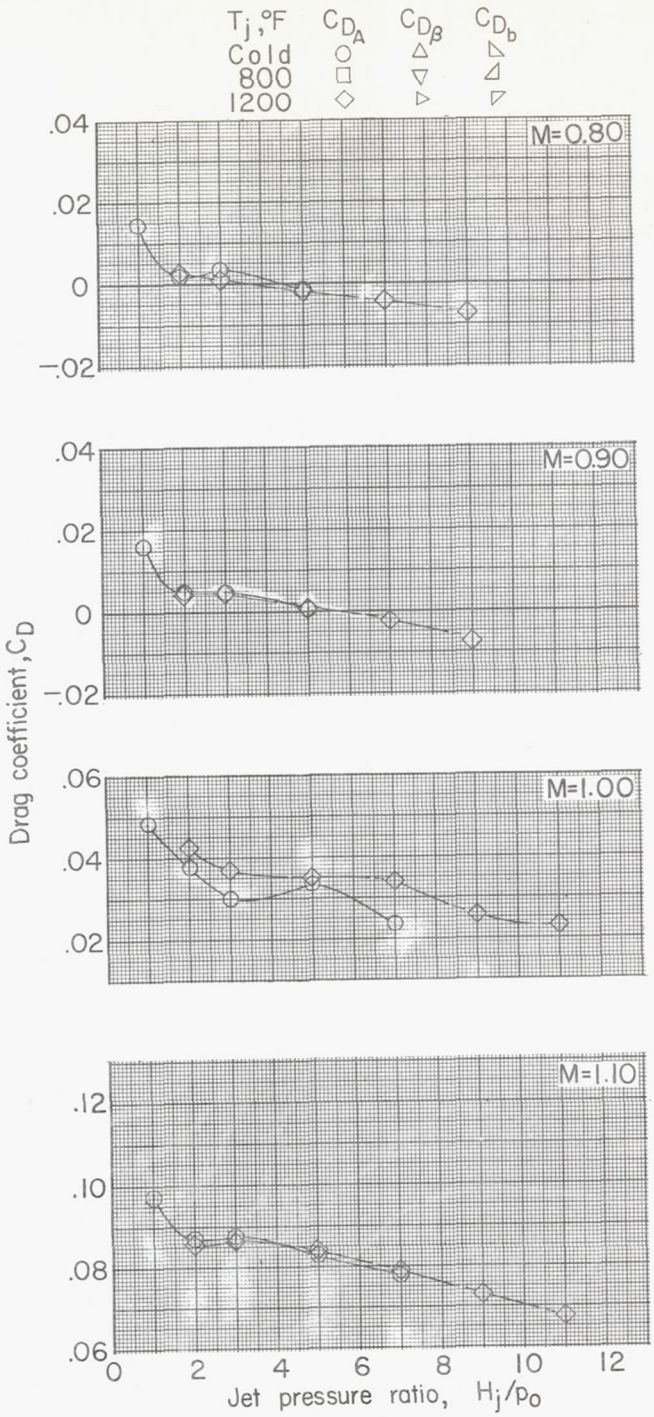

(a) Afterbody IE. $D_j/D_m = 0.248$; $D_j/D_b = 1.000$; $\beta = 16^\circ$.

Figure 6.- Variation of base, boattail, and total afterbody pressure-drag coefficient with jet pressure ratio for different values of jet temperature and stream Mach number.

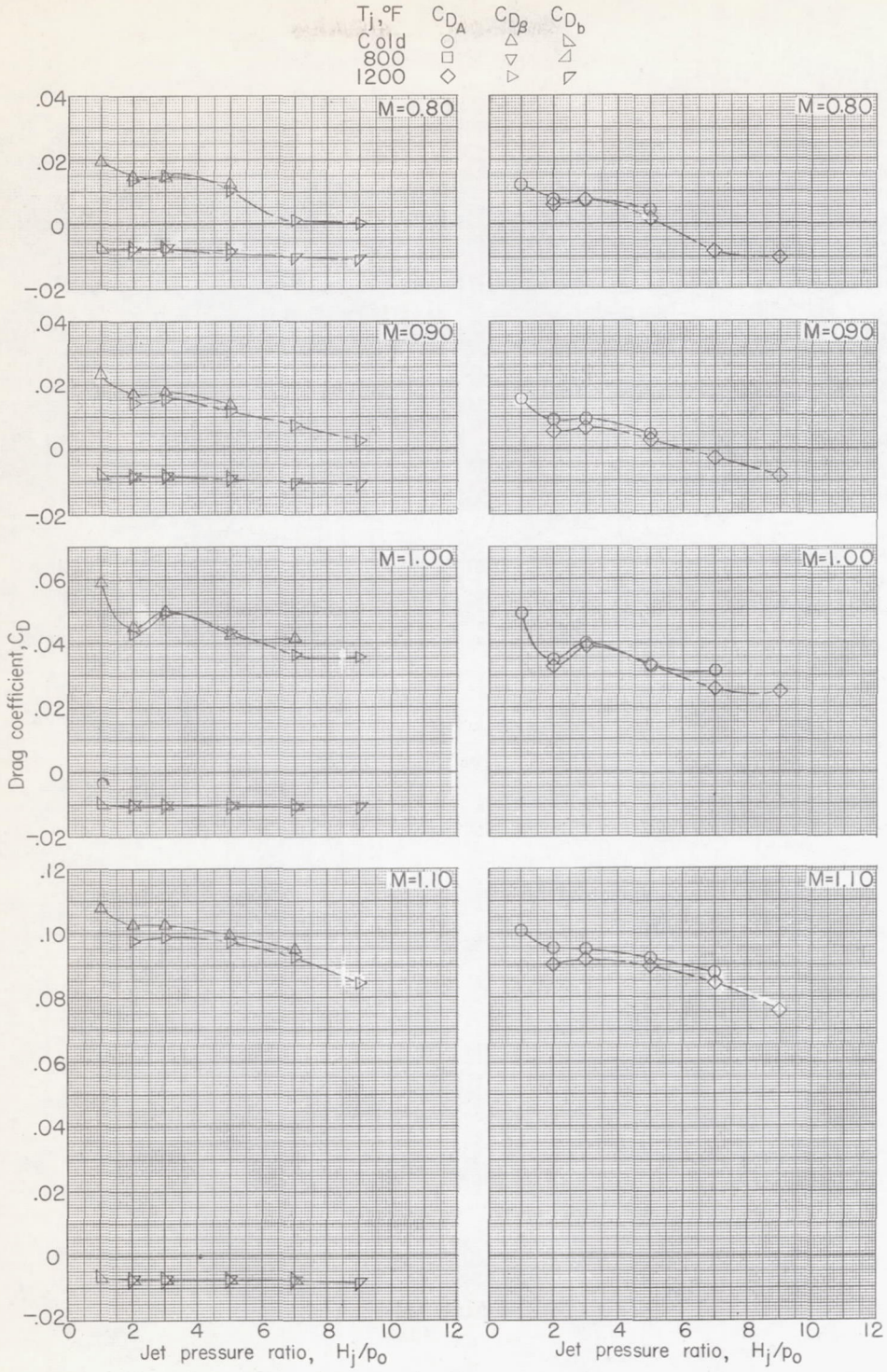

(b) Afterbody I. $D_j/D_m = 0.248$; $D_j/D_b = 0.742$; $\beta = 16^\circ$.

Figure 6.- Continued.

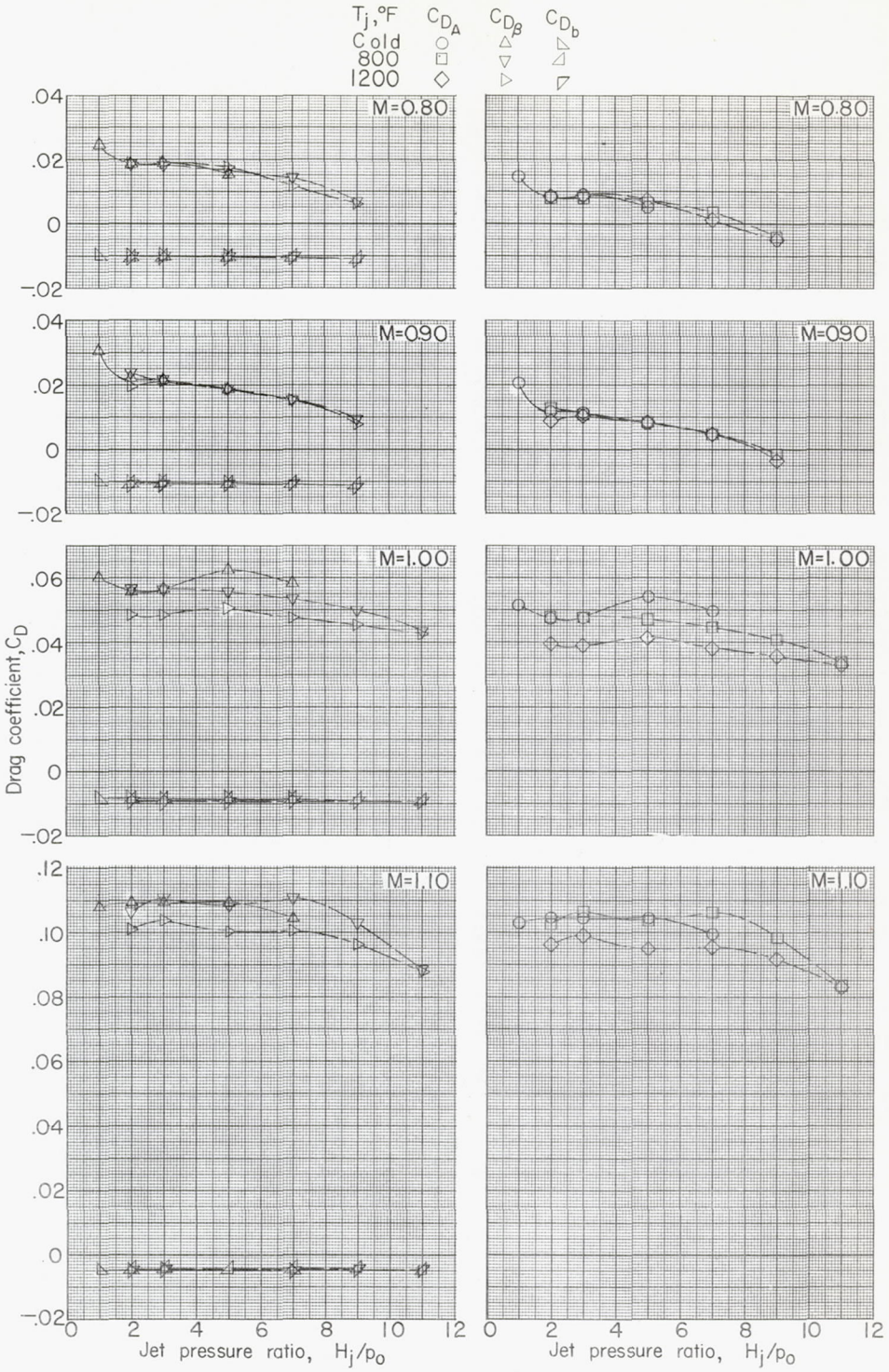

(c) Afterbody II. $D_j/D_m = 0.248$; $D_j/D_b = 0.742$; $\beta = 24^\circ$.

Figure 6.- Continued.

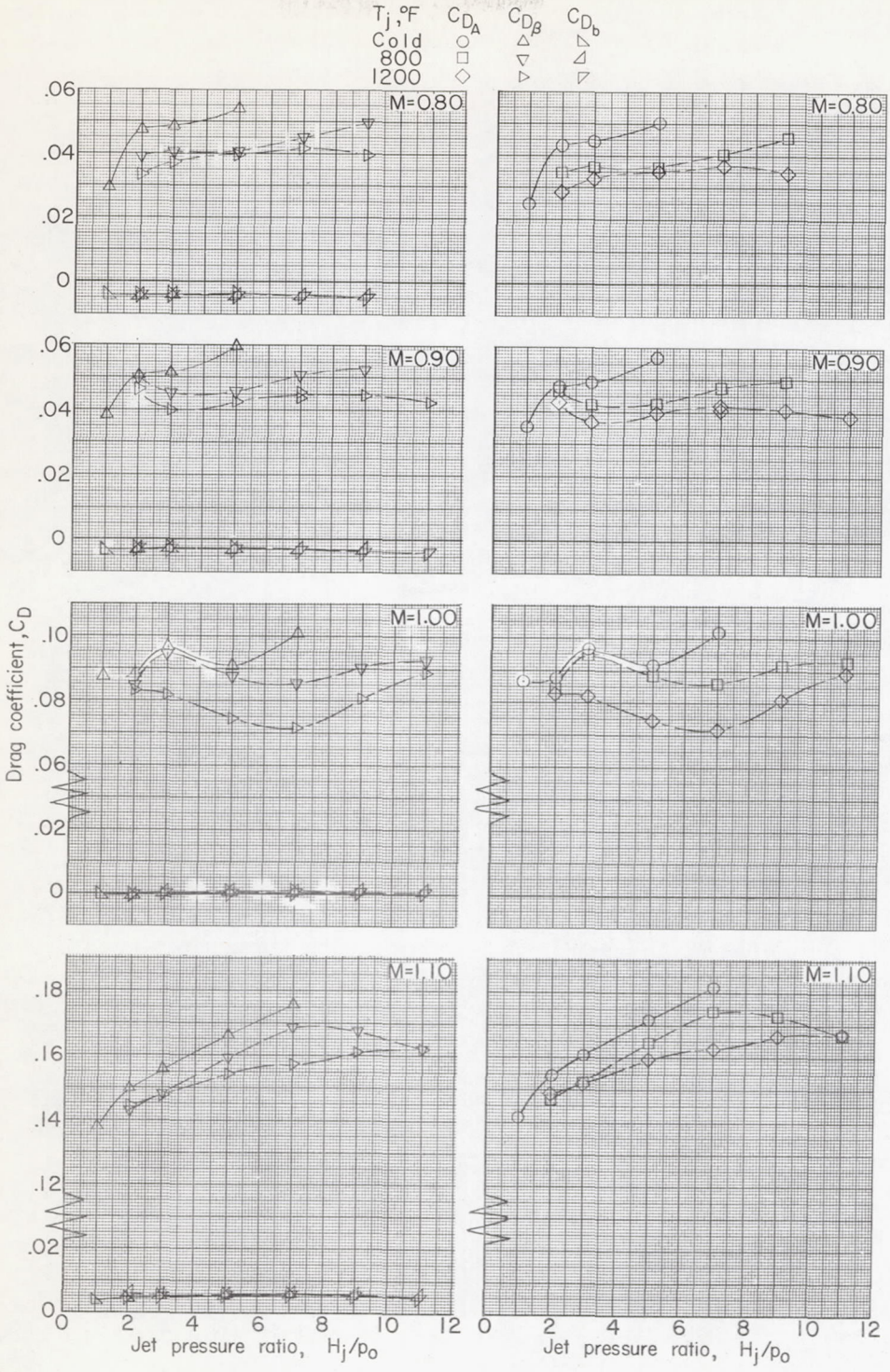

(d) Afterbody III. $D_j/D_m = 0.248$; $D_j/D_b = 0.742$; $\beta = 45^o$.

Figure 6.- Continued.

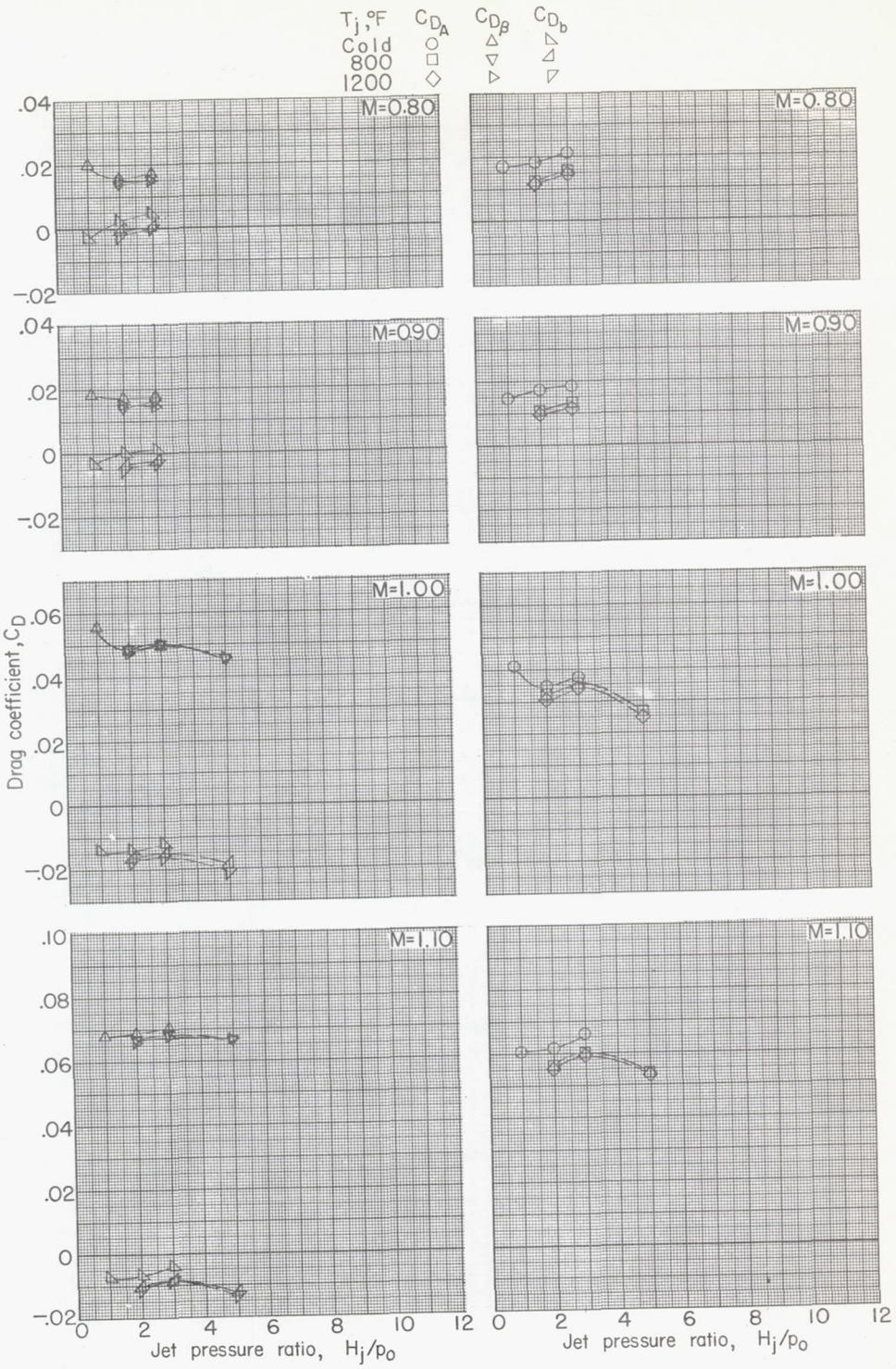

(e) Afterbody IX. $D_j/D_m = 0.351$; $D_j/D_b = 0.698$; $\beta = 7.7^\circ$.

Figure 6.- Continued.

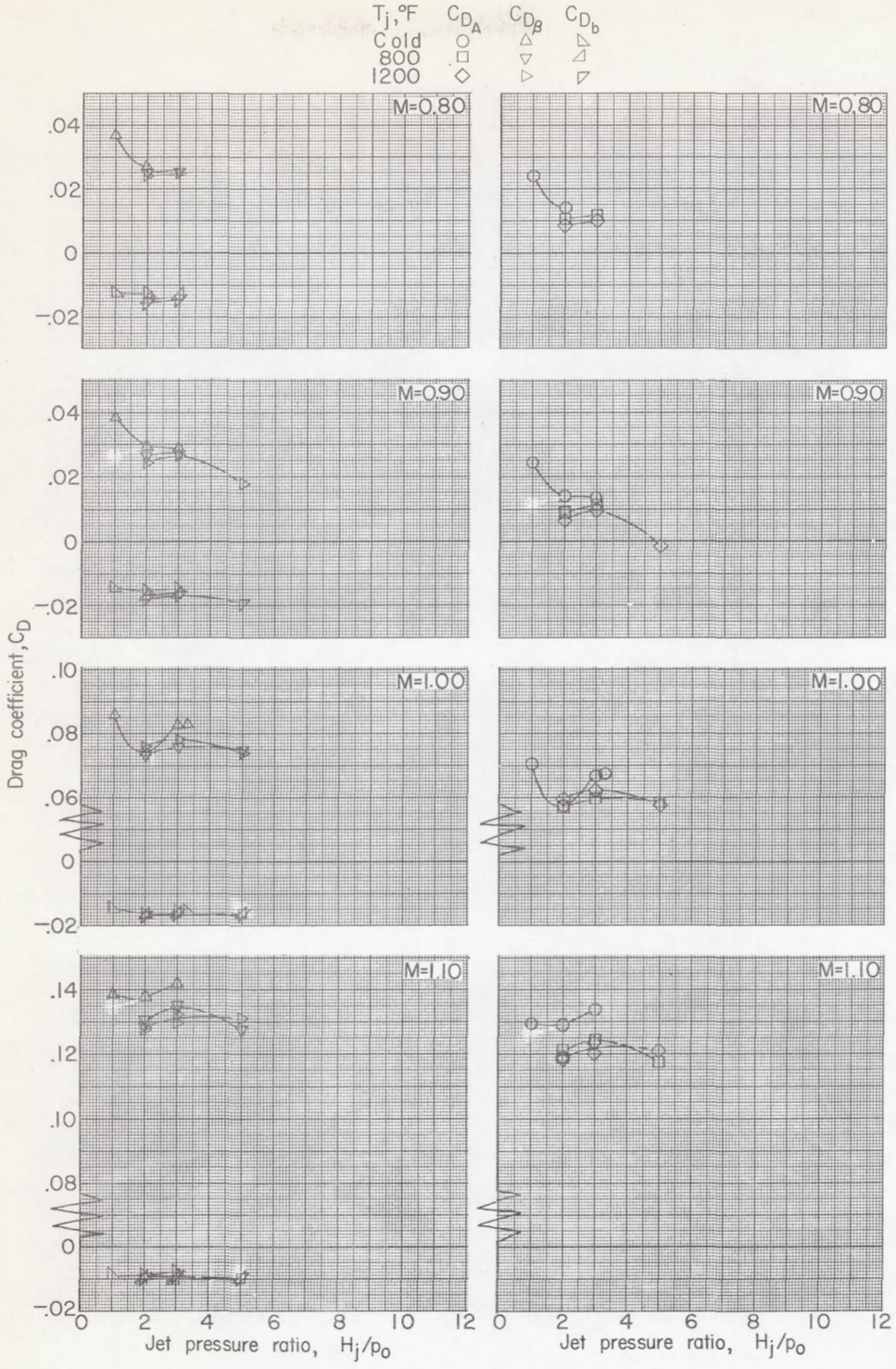

(f) Afterbody IV. $D_j/D_m = 0.351$; $D_j/D_b = 0.742$; $\beta = 16^o$.

Figure 6.- Continued.

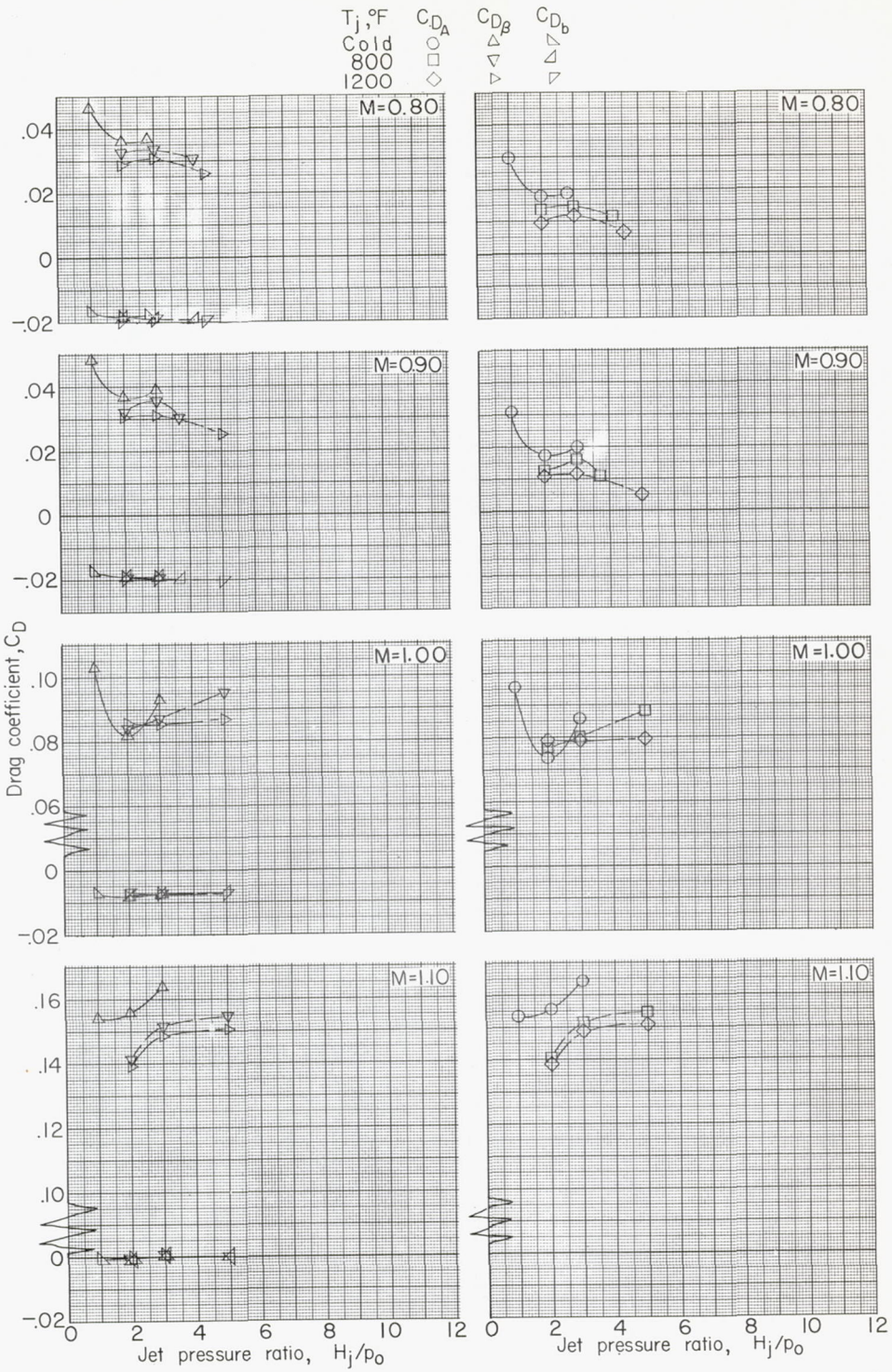

(g) Afterbody V. $D_j/D_m = 0.351$; $D_j/D_b = 0.742$; $\beta = 24^\circ$.

Figure 6.- Continued.

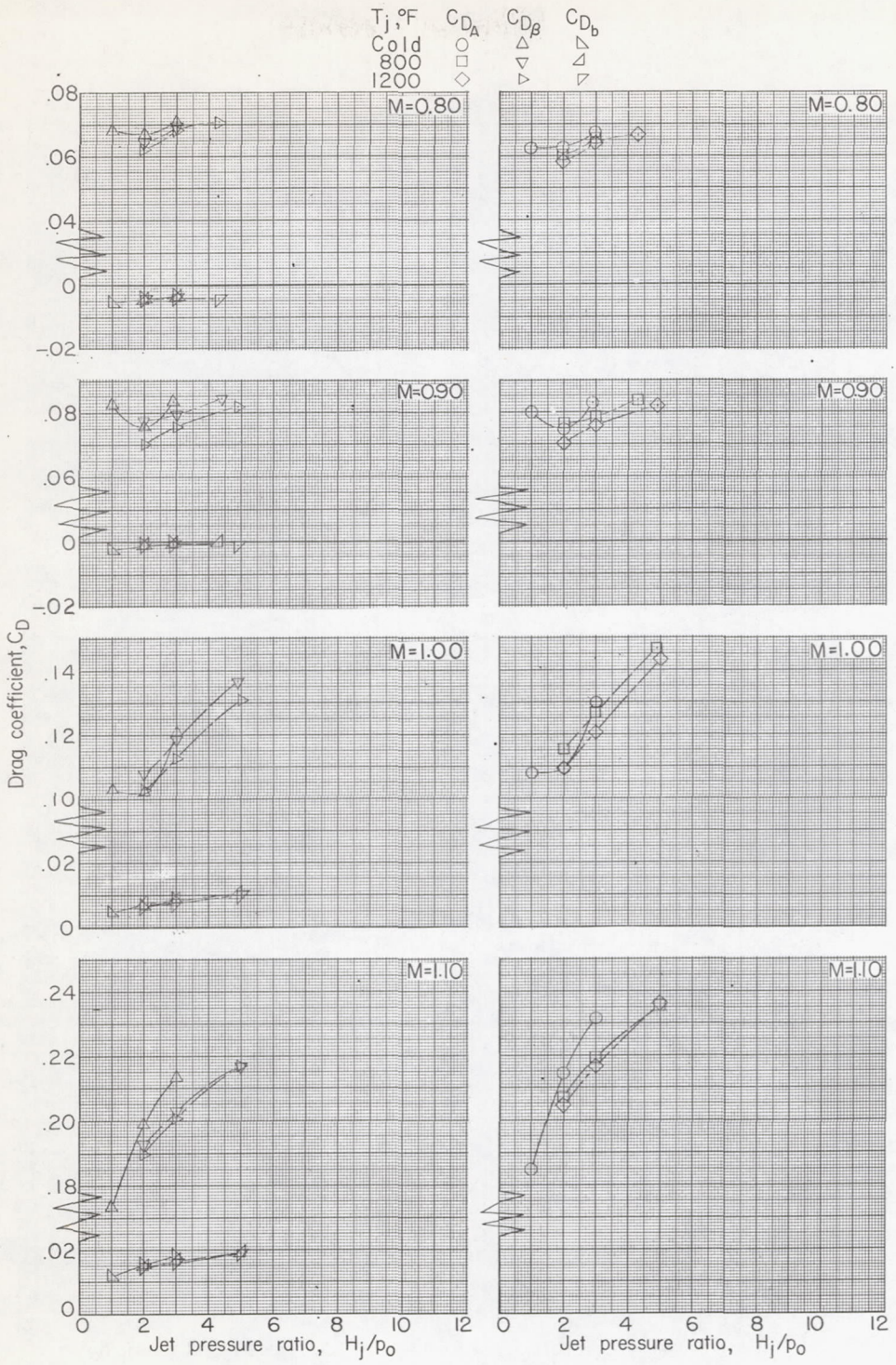

(h) Afterbody VI. $D_j/D_m = 0.351$; $D_j/D_b = 0.742$; $\beta = 45°$.

Figure 6.- Continued.

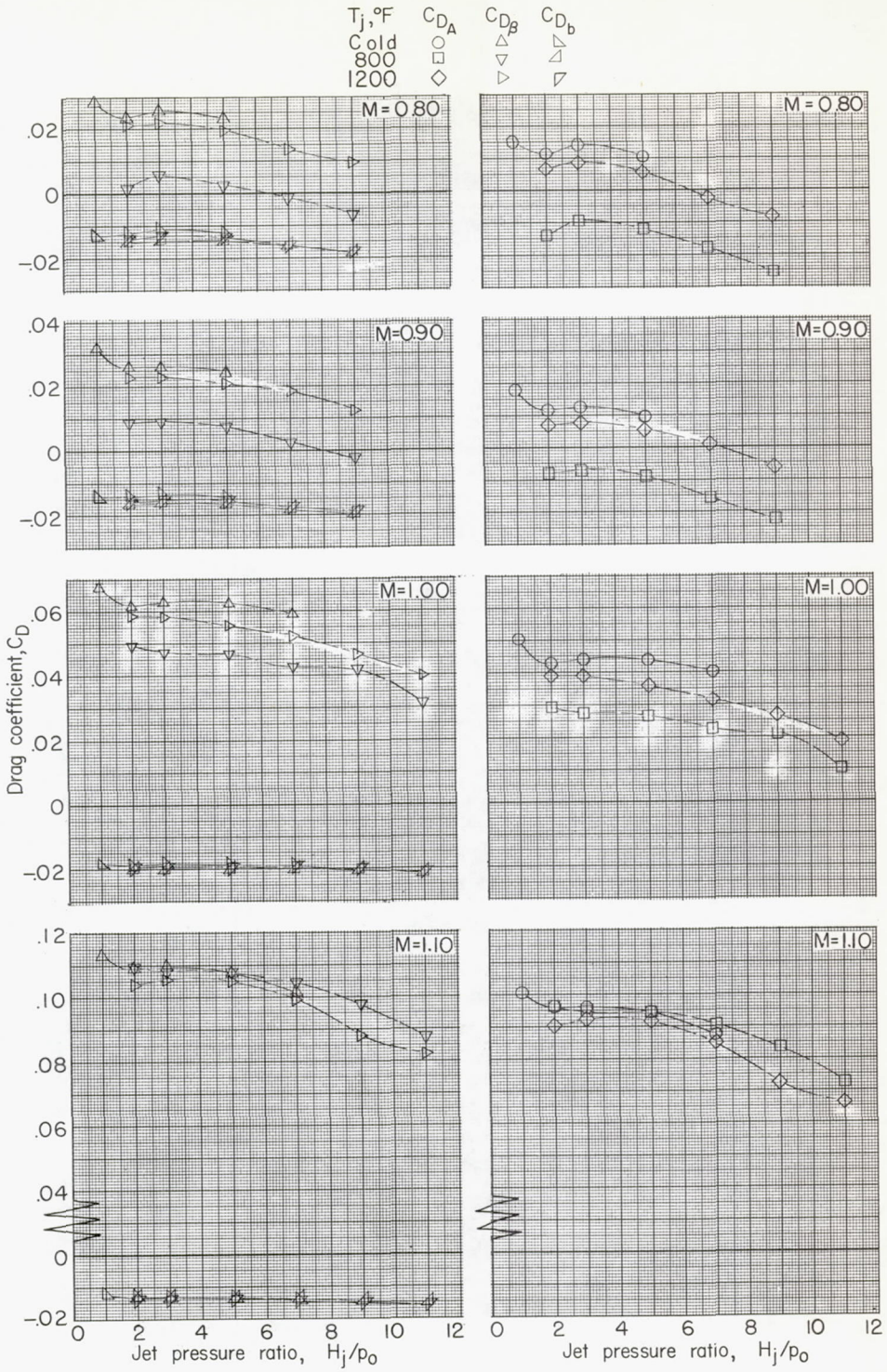

(i) Afterbody VII. $D_j/D_m = 0.248$; $D_j/D_b = 0.643$; $\beta = 16^\circ$.

Figure 6.- Continued.

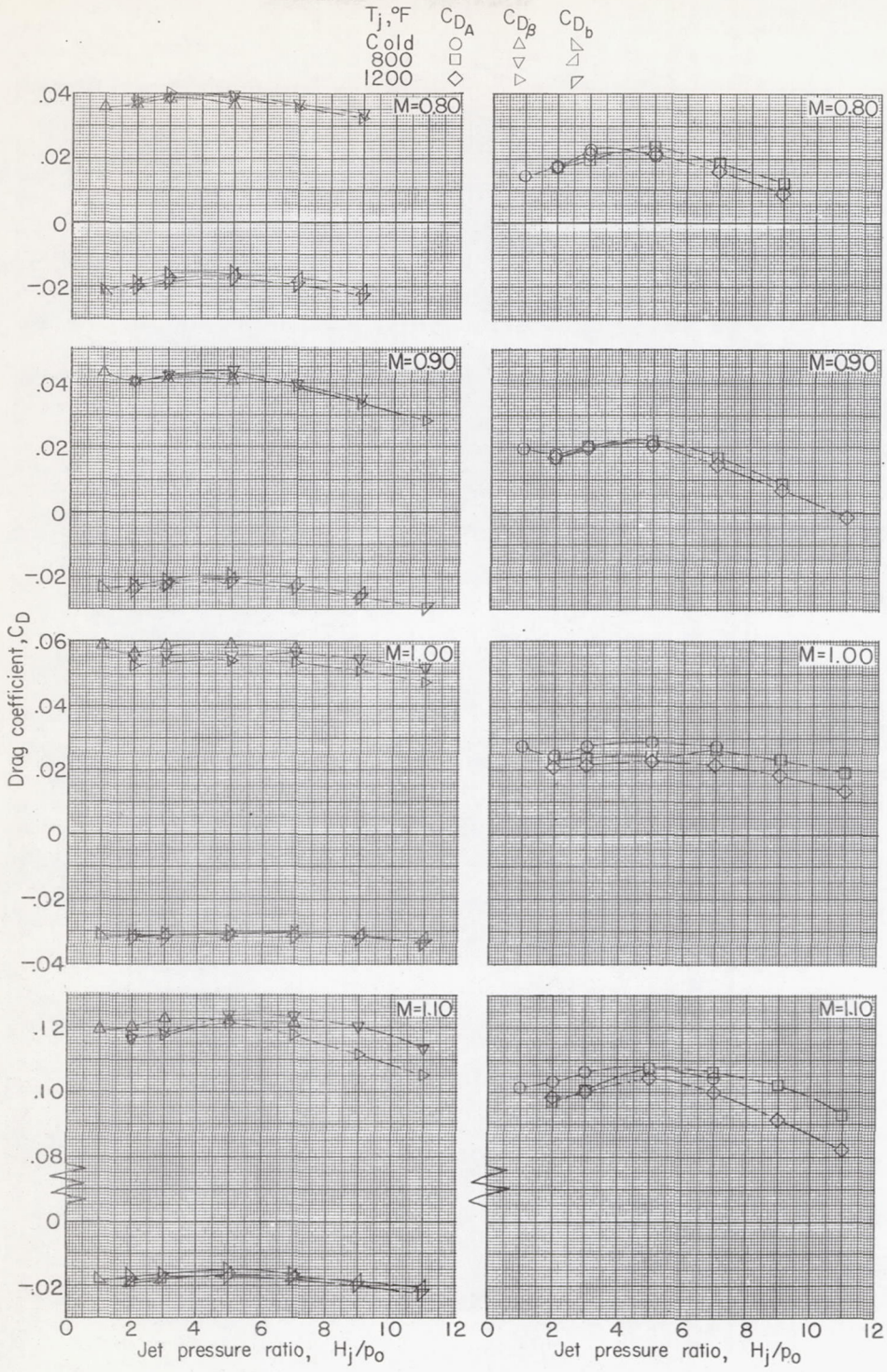

(j) Afterbody VIII. $D_j/D_m = 0.248$; $D_j/D_b = 0.525$; $\beta = 16°$.

Figure 6.- Concluded.